

Study of multi-source image classification algorithms, decomposed data and its combinations for a region in the Amazonia

Etores Marcari Jr.¹
Naiallen Caroline Carvalho¹

¹ Instituto Nacional de Pesquisas Espaciais – INPE
Caixa Postal 515 – 12245-970 – São José dos Campos - SP, Brasil
etore@dpi.inpe.br, naiallen@yahoo.com.br

Abstract. This paper investigates the fusion of several kinds of SAR (Synthetic Aperture Radar) images with optical images, which were used as inputs for land cover classification. Once the images are from different sources, it must be corrected and referenced one over the other. The technique applied to perform the fusion was the classical IHS (Intensity-Hue-Saturation), where the I component was replaced by a product of polarimetric SAR images, that include: HH and HV polarization amplitude SAR image, the ratio of HV to HH amplitudes, the bands ratio and the Freeman-Durden Decomposition components. After fusing, all real images were classified by region growing method using the Bhattacharya distance. The complex image, i. e., SAR images, were classified by the same method, but using the Wishart distribution and the Bhattacharya distance. The classification accuracy of each method was measured by the Kappa coefficient.

Keywords: image fusion, classification, sar fusão de imagens, classificação, sar

1. Introduction

With the availability of multi-source, multi-temporal, multi-resolution and multi-frequency image data from operational Earth observation satellites, the fusion of digital image data has become a valuable tool in the remote sensing image evaluation (POHL; GENDEREN, 1998).

The sensors used in the image acquisition process can be grouped according to the range of the electromagnetic spectrum in which they operate (BRAGA; SANT'ANNA; FREITAS, 2015). The optical sensors operate in the range of 0,3 to 1,5 μ m, and the SAR sensor, in the microwave range - usually between Ka-band(1.5 cm) and P-band (100 cm).

Multi-sensor or multi-source image processing is a method for alignment of images acquired by sensors of different modalities (IRANI; ANANDAN, 1998).

Many studies that combine SAR and optical images have been published as Braga, Sant'Anna e Freitas (2015), Riedel, Thiel e Schmillius (2007), Pereira (2012). However, most of them concern in the use of amplitude SAR image and SAR parameters as the ratio of VV to HH backscatter, the ratio of HV to HH backscatter, the phase difference between HH and VV, and the correlation between HH and VV. In this work we propose the use of the information extracted from the Freeman–Durden decomposition as an additional information plan to be used in the IHS fusion and the Cloude–Pottier decomposition, to determine the classes.

2. SAR Images

The radar images are formed by radar echoes of various combinations of transmitting and receiving polarizations from scattering media (LEE; POTTIER, 2009). And the SAR images are obtained from satellites such as ERS, JERS, ALOS, RADASAT.

The main difference between optical and microwave images is the way each one interacts with the targets: while in the optical case the images are formed by incoherent interaction, SAR images are formed by coherent interaction, that means the information of phase is very

important. Due to the coherent interference of waves reflected from many elementary scatterers, the speckle appears in this images.

The speckle effect causes the granular noise pattern, and therefore, a pixel-to-pixel variation in the intensities (LEE; POTTIER, 2009). This effect turns the image analysis harder and reduces the effectiveness of the image segmentation and classification. According to Lee e Pottier (2009), a common approach to speckle reduction is done by filtering or by multi-look processing. In this paper, a boxcar filter to speckle noise reducing is applied.

3. Images Attributes

3.1. Optical Attributes

A large number of attributes can be extracted from optical images. Despite this, only the combination of gray levels taken from three bands of the Landsat-5 satellite (2,4,5) was used as input of a classification scenario.

3.2. SAR Polarimetric Attributes

The PALSAR full polarimetric sensors are able to transmit and receive both the orthogonal components (H and V). Therefore, phase difference, amplitude product and amplitude ratio between two or more polarizations attributes can be created.

These attributes are important discriminators for terrain classification and geophysical parameter estimation (LEE; POTTIER, 2009). Pereira (2012) introduces different ways to extract attributes from polarimetric images and shows why they should be used. Based on that, two kinds of attributes are chosen: band ratios and Principal Components.

3.3. Bands Ratios

In this paper, two kinds of bands ratios were used: HV/HH and NL. The first one highlights the features which elements are predominantly in the vertical direction, which vegetation types can be distinguished, and has a high sensibility for volumetric scattering. The second ratio is computed as shown below:

$$NL = \frac{HH \times HV}{HH + HV} \quad (1)$$

This ratio allows the use of the combined information taken from bands HH and HV, when applying the fusion process of optical and SAR images.

3.4. Principal Components

The PC (Principal Components) extraction applied on an original set of bands aims the creation of new, linearly uncorrelated, bands. In this work, the first component is used as a classification attribute. When using only the first component, the dimensionality of the data is reduced. The PC are extracted using as input the covariance matrices.

The PCA (Principal Components Analysis) follows the method proposed onto (RICHARDS, 1999), and was applied to the Amplitude HH and HV components.

3.5. SAR Decompositions

The purpose of a decomposition in radar polarimetry is to provide means for interpretation and optimum utilization of polarimetric scattering. Here, the Incoherent Target Decomposition were used because most of the targets in the environment are incoherent and have random scattering, therefore they are studied in the statistical perspective, using as base the covariance matrix $[C]$ and the coherency matrix $[T]$.

The two method of incoherent target decomposition used were: the Freeman-Durden and the Cloude-Pottier decomposition.

3.5.1. Cloude-Pottier

The Cloude-Pottier decomposition consists in the evaluation of the eigenvalues and the eigenvector taken from the matrix $[T]$ and through it, determine the polarimetric SAR parameters such as Entropy (H), Alpha Angle (α) and the Anisotropy (CLOUDE; POTTIER, 1997), expressed by the Equation 2.

$$H = \sum_{i=1}^3 (-P_i \log_3 P_i), \quad \alpha = \sum_{i=1}^3 (P_i \cos^{-1}(k_{xi})), \quad A = \frac{\lambda_2 - \lambda_3}{\lambda_2 + \lambda_3} \quad (2)$$

where λ_i are the eigenvalues of $[T]$, k_{xi} is first element of eigenvector associated to λ_i and $P_i = \frac{\lambda_i}{\lambda_1 + \lambda_2 + \lambda_3}$.

The alpha parameter has a range from 0 to 90 degrees and it is an average representation of the eigenvector information while the entropy lies between 0 and 1 and represents the eigenvalue information. The anisotropy also lies between 0 and 1 and has suggested as a new feature to distinguish depolarizing mechanisms in surface and volume scattering (CLOUDE; POTTIER; BOERNER, 2002).

The classes used for the classification process was determined by the Cloude-Pottier decomposition.

3.5.2. Freeman-Durden

The Freeman-Durden decomposition is a technique based on physical models, which goal is estimated the contribution of canonical components to the total backscatter of SAR images, without utilizing any ground truth measurements.

The three scattering mechanism components included in the model are canopy scatter from randomly oriented dipoles (volumetric), first-order Bragg surface scattering, and a double-bounce scattering mechanism (FREEMAN; DURDEN, 1998). According to Freeman e Durden (1998), the total backscatter can be expressed as the sum of the statistics for the individual mechanisms (Equation 3).

$$P = P_s + P_d + P_v \quad (3)$$

were P_s , P_d and P_v are the surface, double-bounce, and volume (or canopy) scatter contributions.

4. Methodology

This section contains a description of the work methodology, including the pre-processing steps, the applied fusion method, and the classification methods and scenarios.

4.1. Image pre-processing

Image pre-processing can significantly increase the reliability of a classification. Several operations which intensify or reduce certain image details enable a better evaluation.

When combining and fusing any kind of images (in this case, optical and radar ones), it is assumed that they have the same projection and the same geographic coordinates system. The register between them is also very important (if possible, with sub-pixel precision).

Due to the format of the acquired ALOS/PALSAR images, some extra steps are necessary (Figure 1). After that, the images are registered, trying to acquire sub-pixel precision. So the images are prepared for the main processing steps.

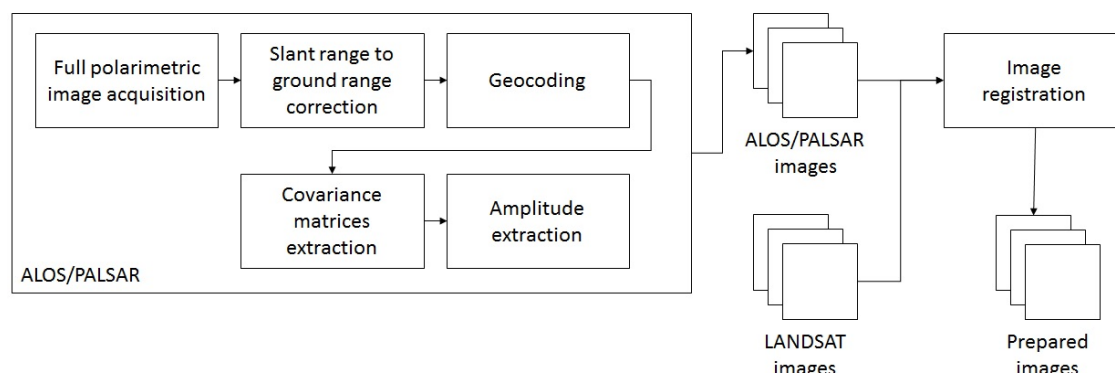


Figure 1: Pre-processing steps.

4.2. The IHS transformation

The IHS transformation is related to the perception of the human being about colors. Here, "I" refers to the intensity or brightness, "H" is the hue and "S" saturation (how the color is pure).

The fusion of optical and SAR data is done by choosing three optical bands, selected according the study/work objective and transforming them from the RGB space to the IHS space. At this space, the color and intensity are separated.

The intensity, related to the surface roughness, is changed by the SAR selected image, and the back to the RGB space is performed. The conversion is presented in Equation (4).

$$\begin{bmatrix} R \\ G \\ B \end{bmatrix} \xrightarrow{\tau} \begin{bmatrix} I \\ H \\ S \end{bmatrix} \xrightarrow{\zeta} \begin{bmatrix} SAR \\ H \\ S \end{bmatrix} \xrightarrow{\tau^{-1}} \begin{bmatrix} R_{new} \\ G_{new} \\ B_{new} \end{bmatrix} \quad (4)$$

4.3. Scenarios

From the selected attributes presented previously, eight scenarios were created. The Table 1 shows its characteristics. The combinations between SAR and optical images were made by using the IHS transformation, which the "I" component was changed by the SAR attribute or its decomposition.

Table 1: Scenarios list.

Acronym	Characteristic
RGB	normal composition with R(5), G(4) and B(2)
FullPol	covariance matrix taken from full polarimetric data
RGB + PC1	RGB and SAR First PC
RGB + DIV	RGB and SAR DIV
RGB + NL	RGB and SAR NL
RGB + SUP	RGB and Freeman-Durden Superficial decomposition
RGB + VOL	RGB and Freeman-Durden Volumetric decomposition
RGB + DB	RGB and Freeman-Durden Double-Bounce decomposition

5. Classification

5.1. Selected Classes

An unsupervised classification scheme for polarimetric image SAR based on the use of the $H - \alpha$ plane, proposed by Cloude and Pottier was applied to discover and select the classes used as input to classification analysis. This plan is subdivided into eight basic zones characteristic of classes of different scattering behavior. For this analysis, the central pixel for each zone was taken from the zone in the plane, as shown in Figure 2a.

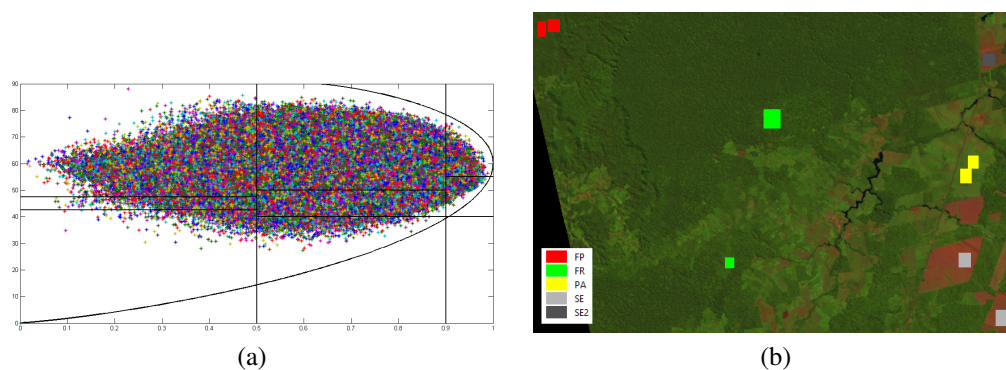


Figure 2: a) Classes samples in the Cloude-Pottier plan. b) Classes samples over the LANDSAT image. FP(Native Forest), FR(Reforestation), PA(Pasture), SF(Bare Soil), SF2(Bare Soil 2).

5.2. Method

After the class definition, acquisition and testing samples were extracted from the image (Figure 2b). Both kinds of images (real and complex) were classified by region growing method using the Bhattacharya distance. The difference is in the distribution used in data modeling: The real images were modeled by the Gaussian distribution, and the complex one, by the Wishart. The classification was performed for all the scenarios. After that, the global Kappa coefficients were computed, and the results are presented in the next section.

The processing related to SAR image, as decompositions and Wishart classification, as well as the confusion matrix and kappa coefficient were implemented in C++, using the TerraLib library, and in IDL language. The other process were done in Spring software, both created and supported by DPI/INPE (Image Processing Division - Brazilian Institute for Space Research).

6. Results

The next figures present the result of the classification for all scenarios. The red circles indicate areas which classifier was unable to classify. The data produced by (BRAGA; SANT'ANNA; FREITAS, 2015) is used as ground truth, due to the in-situ validation, performed by its working team. Using this data, the Kappa's coefficient was computed for each classification result.

The classification of FullPol scenario could not separate the Native Forest and Reforestation classes correctly, and could not classify the second type of bare soil. Its Kappa was the worst one.

As Figure 3b shows, despite having the highest kappa's value, the result of the optical image classification has lot of area without classification.

The classification from the RGB+PC1 scenario (Figure 3c) still have some non-classified areas (less than the RGB ones) and has the bigger kappa's coefficient result. When visually compared to the input image (visual interpretation), it seems a good result.

The result of RGB+DIV and RGB+NL scenarios (Figures 3d and 3e) have good kappa values and good behavior when classifying the forest classes. Both scenarios presented confusion when classifying bare soil and pasture.

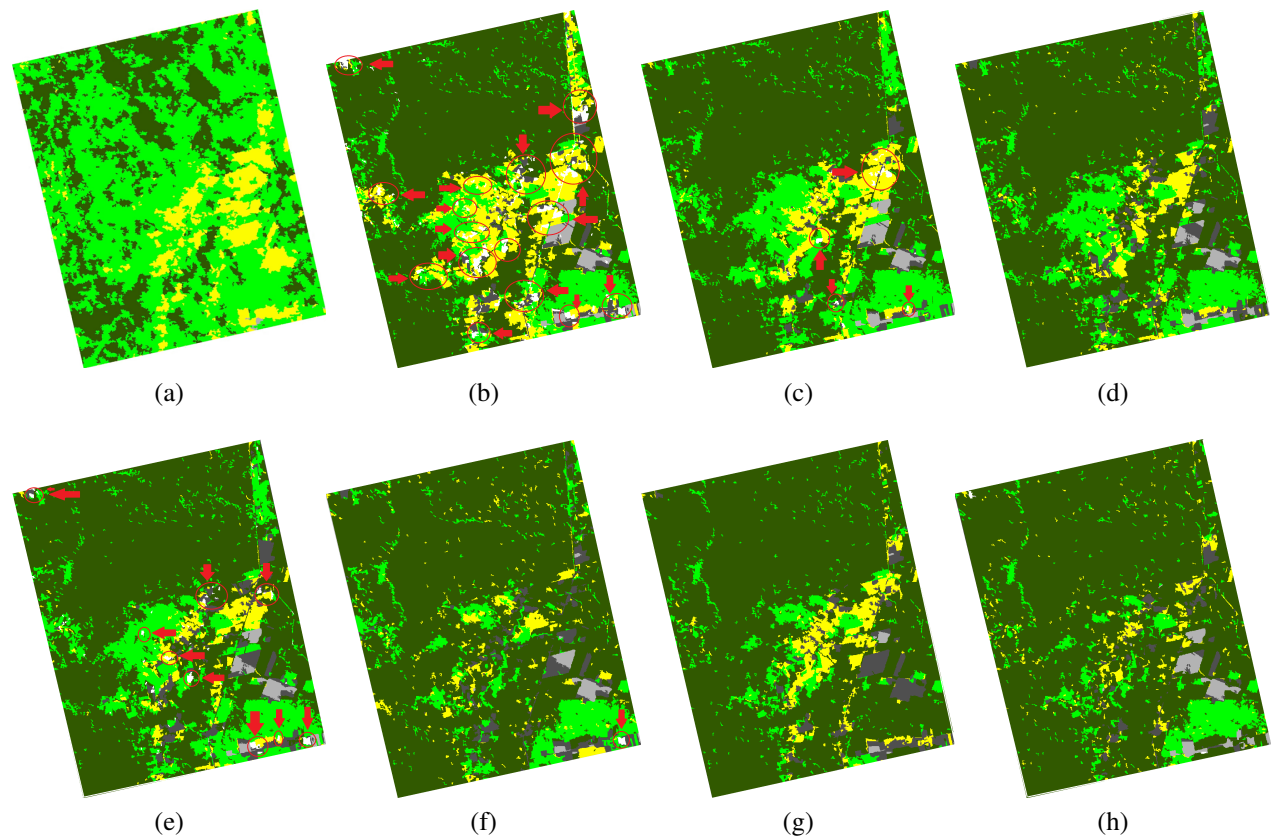


Figure 3: Classification of: a) Polarimetric SAR image. b) RGB image, only optics images. c) RGB and SAR First PC. d)RGB and SAR DIV. e)RGB and SAR NL. f)RGB and Freeman-Durden Superficial decomposition. g) RGB and Freeman-Durden Volumetric decomposition. h)RGB and Freeman-Durden Double-Bounce decomposition.

As expected, the RGB+SUP scenario, instead of a non-high kappa value, produced a good result when identifying the two kinds of bare soil.

The RGB+VOL scenario has a low Kappa's value, and its result is expected, due to some specific characteristics (presented in the following section).

The worst Kappa value of the real images was produced by the RGB+DB scenario. Apart from this result, it produced better classification for Reforestation when compared to RGB-VOL.

7. Conclusion

From the analysis presented above, we can conclude that the multi-source image classification, including decomposed data, is practicable. Instead of low kappa values, the components can be applied to the specific target classification.

The low Kappa and classification quality problems, presented by the FullPol images, can be explained by the high interval between the dates of the image acquisition and the in-situ

Table 2: Kappa coefficient result.

Image	Kappa	Variance	z
RGB	0.9811	0.0001	86.1711
FullPol	0.2590	0.0001	28.9341
RGB + PC1	0.9977	0.0001	93.7007
RGB + DIV	0.8226	0.0001	72.0016
RGB + NL	0.9127	0.0001	84.1898
RGB + SUP	0.7840	0.0001	70.0340
RGB + VOL	0.5000	0.0002	37.1231
RGB + DB	0.4858	0.0001	40.5150

validation. For better results, a new image should be acquired.

The confusion between the two kinds of forest, presented in the RGB+VOL scenario, is expected because the scattering behavior is almost the same for both cases. The confusion between pasture and forest is due to the "size of the pasture elements": depending on its size, it results in a Volumetric behavior, causing the confusion. And the data taken from the L-band (ALOS/PALSAR data) can present behavior as presented before.

The RGB+DB scenario, apart from its result, it produced better classification for Reforestation when compared to RGB-VOL. It happens because there are more tree trunks in this type of area, producing the double-bounce behavior.

As presented in this paper, different kinds of data fusioning and combination can be used for classification, but for specific cases, and for specific areas. Depending on the aim of classification, some combinations can present better results when compared to others.

References

- BRAGA, B. C.; SANT'ANNA, S. J. S.; FREITAS, C. d. C. Stochastic distances and uncertainties maps applied to multisources data classification. *Revista Brasileira de Cartografia*, SBC, v. 67, n. 7, p. 1391–1411, 2015.
- CLOUDE, S. R.; POTTIER, E. An entropy based classification scheme for land applications of polarimetric sar. *IEEE Transactions on Geoscience and Remote Sensing*, IEEE, v. 35, n. 1, p. 68–78, 1997.
- CLOUDE, S. R.; POTTIER, E.; BOERNER, W. M. Unsupervised image classification using the entropy/alpha/anisotropy method in radar polarimetry. In: *NASA-JPL, AIRSAR-02 Workshop*. [S.l.: s.n.], 2002. p. 04–06.
- FREEMAN, A.; DURDEN, S. L. A three-component scattering model for polarimetric sar data. *IEEE Transactions on Geoscience and Remote Sensing*, IEEE, v. 36, n. 3, p. 963–973, 1998.
- IRANI, M.; ANANDAN, P. Robust multi-sensor image alignment. In: *IEEE. Computer Vision, 1998. Sixth International Conference on*. [S.l.], 1998. p. 959–966.
- LEE, J.-S.; POTTIER, E. *Polarimetric radar imaging: from basics to applications*. [S.l.]: CRC press, 2009.
- PEREIRA, L. d. O. *Avaliação de métodos de integração de imagens ópticas e de radar para classificação do uso e cobertura da Terra na região Amazônica*. Dissertação (Mestrado) — Instituto Nacional de Pesquisas Espaciais - INPE, São José dos Campos - SP - Brasil, 2012.



POHL, C.; GENDEREN, J. L. V. Review article multisensor image fusion in remote sensing: concepts, methods and applications. *International journal of remote sensing*, Taylor & Francis, v. 19, n. 5, p. 823–854, 1998.

RICHARDS, J. *Remote Sensing Digital Image Analysis: An Introduction*. [S.l.]: Springer-Verlag, 1999.

RIEDEL, T.; THIEL, C.; SCHMULLIUS, C. Fusion of optical and sar satellite data for improved land cover mapping in agricultural areas. In: . [S.l.: s.n.], 2007.